Atmos. Chem. Phys. Discuss., 13, 903–933, 2013
www.atmos-chem-phys-discuss.net/13/903/2013/
doi:10.5194/acpd-13-903-2013

Atmospheric Chemistry and Physics Discussions

Analysis of a winter regional haze event and its formation mechanism in the North China Plain

X. J. Zhao, P. S. Zhao, J. Xu, W. Meng, W. W. Pu, F. Dong, D. He, and Q. F. Shi

Institute of Urban Meteorology, Chinese Meteorological Administration, Beijing 100089, China

Received: 9 November 2012 – Accepted: 19 December 2012 – Published: 9 January 2013

Correspondence to: X. J. Zhao (xjzhao@ium.cn)

Published by Copernicus Publications on behalf of the European Geosciences Union.

Abstract

A regional haze episode occurred in the Beijing, Tianjin and Hebei province (BTH) area in the North China Plain (NCP) from 16 to 19 January 2010. The chemical and optical properties of aerosols and the meteorological condition were investigated in this study with intensive measurement of aerosol and trace gases from 14 to 23 January 2010 at five sites. The episode was caused by the combination of anthropogenic emissions and surface air stagnation under a high pressure system followed by a low pressure system. The concentrations of $PM_{2.5}$ and trace gases increased significantly on a regional scale during this episode. The increased aerosol scattering coefficient (σ_{sp}), absorption coefficient (σ_{ap}), and aerosol optical depth (AOD) showed the importance of aerosol extinction during this haze episode. The increase of secondary inorganic pollutants (SO_4^{2-}, NO_3^-, NH_4^+) was observed simultaneously at four sites, especially in the plain area of BTH, which could be identified as a common characteristic of pollution haze in east China. The organic matter (OM) was different from secondary inorganic pollutants, which increased more significantly at Chengde (CD) site than the other three sites in plain area. The sulfate and nitrate in $PM_{2.5}$ were mainly formed through the heterogeneous reaction process in the urban area. The secondary organic aerosols in $PM_{2.5}$ only existed during haze days at CD but in both haze and normal days at the other three sites. The chemical characteristics of aerosols in $PM_{2.5}$ indicated that the secondary formation of aerosol was one important mechanism in the formation of haze episode. The strong temperature inversion and descending air motions in the planetary boundary layer (PBL) allowed pollutants to accumulate in a shallow layer. The weak surface wind speed produced high pollutants concentration within these source regions. The accumulation of pollutants was one main factor in the haze formation. The enhanced southwest wind in the last period of this episode transported pollutants to the downwind area and expanded the regional scope of the haze.

ACPD
13, 903–933, 2013

1 Introduction

China has undergone very rapid economic growth since the economic reforms began in 1978 and this has resulted in an increase in energy consumption, air pollution and associated health effects. In China large emissions were concentrated in the mega-city clusters, such as BTH, the Pearl River Delta (PRD) and the Yangtze River Delta (YRD) regions (Parrish and Zhu, 2009). The BTH is one region in north China in which the economic development is most active. It consists of two municipalities Beijing and Tianjing, the capital city Shijiazhuang and other six cities of Hebei province. Chengde is one of the six cities and located in the northern mountainous area of Hebei.

With the rapid economic development, population expansion and urbanization, BTH region has been experiencing severe air pollution problem, especially aerosol pollution. The decrease of visibility is one of the most notable effects of aerosol. In BTH region, the visibility showed a decreasing trend during 1980–2008 and haze days increased after the 1990s (Zhao et al., 2011a). In urban area, haze days usually company with severe air pollution. Numerous field studies provide abundant information about concentrations, compositions, source and optical properties of aerosol particles in major cities and other areas in BTH. By comparing the different chemical characteristics of aerosols in dust, haze, and clear days in Beijing, Wang et al. (2005) pointed out that $(NH_4)_2SO_4$, NH_4NO_3, and $Ca(NO_3)_2$ were the major species on haze days in spring. Sun et al. (2006) investigated the chemical characteristics of $PM_{2.5}$ and PM_{10} in haze–fog episodes in Beijing and found that the concentrations of elements and water-soluble ions in haze–fog episodes were more than 10 times higher than those on non-episode days. The serious air pollution in haze-fog episodes was strongly correlated with the meteorological conditions and the emissions of pollutants from anthropogenic sources. With analysis of the phase and mixing state of individual aerosol particles, Li et al. (2010) found that the agricultural biomass burning particles were significant contributors to the regional hazes in northern China and prominent in Beijing in June. During haze episodes, the aerosol scattering coefficient increased significantly and

ACPD
13, 903–933, 2013

showed different spatial distribution pattern under different meteorological conditions (Zhao et al., 2011b).

There are many similar studies in other cities and mega-city clusters in China. Li et al. (2011) studied the mixing state of individual particles in Jinan city during a regional haze episode in winter. Their study confirmed that metal-catalyzed oxidation in the aqueous phase was a major pathway of sulfate formation. Huang et al. (2012) discussed the different chemical and optical properties of three haze types in Shanghai. The size distribution of aerosol in a long-lasting haze in Nanjing indicated that aerosol concentration in the diameter range of 0.6 to 1.4 µm increased dramatically and mainly attributed to the remarkable increase of σ_{sp} and decrease of visibility (Kang et al., 2013). In Guangzhou, the particle mass-size distributions were bimodal and dominated by fine particles in haze days (Tan et al., 2009). These studies have provided abundant information about the formation of haze in different aspects. However, few studies have investigated the characteristics and formation of haze in regional scale.

In this study, an intensive field experiment using various techniques was carried out at five sites in BTH during a regional haze episode. The chemical and optical characteristics of the aerosol were analyzed, and the formation of haze from the point of chemical and meteorological process was investigated as well.

2 Methods

2.1 Field observation

2.1.1 Sampling sites and collection

As shown in Fig. 1, five sites were selected in the BTH region. Beijing and Tianjin are two municipalities surrounded by Hebei province. Beijing, Tianjin, and most of Hebei are located in the NCP, which is bordered on the north by the Yanshan Mountains and on the west by the Taihang Mountains edge of the Shanxi plateau. Shangdianzi is a re-

ACPD
13, 903–933, 2013

gional background station, which is 100 km northeast to the urban area of Beijing and located in the boundary of plain area. It is also one of the Global Atmosphere Watch (GAW) stations. A detailed description of the Shangdianzi site has been previously reported (Zhao et al., 2009). Chengde is one city located in the northern mountainous area of Hebei, and outside the NCP region. The four sites were located with the urban areas of Beijing, Tianjin, Shijiazhuang and Chengde, and all monitoring was done on the roofs of local meteorological bureaus. Another sampling site was set at Shangdianzi. In this paper, the sampling sites for Shangdianzi, Beijing, Tianjin, Shijiazhuang and Chengde are abbreviated as SDZ, BJ, TJ, SJZ and CD.

Aerosol samples of $PM_{2.5}$ were collected on 90 mm polypropylene membrane filters and quartz fiber filters using two parallel medium-volume samplers (100 L min^{-1}) at each site. The duration of sampling was generally 24 h. Polypropylene membrane filters were used for analysis of inorganic elements. Quartz fiber filters were used for carbon and water-soluble ions components, and pre-heated at 800 °C for 3 h before using. All of the filters were weighed before and after sampling.

2.1.2 Automatic $PM_{2.5}$ and gases monitor

The real-time mass concentrations of $PM_{2.5}$ were measured by a tapered element oscillating microbalance (Thermo Electron Corporation, TEOM 1400a at BJ and SDZ and 1405D at TJ). Concentrations of sulfur dioxide (SO_2), ozone (O_3) and its precursors (CO, NO, NO_2 and NO_x) at BJ station were observed by a set of commercial instruments from Ecotech, Inc., Australia. The instruments include an EC9810 Ozone analyzer, EC9830 CO analyzer, EC9841 NO_x analyzer and EC9850 SO_2 analyzer. At TJ and SDZ stations, gases were observed by a set of commercial instruments from Thermo Environmental Instrument, Inc., USA. The instruments include a TE49C O_3 analyzer, TE48C CO analyzer, TE 42CTL NO_x analyzer and TE43C SO_2 analyzer. All the measured data were recorded at 5-min intervals.

ACPD
13, 903–933, 2013

2.1.3 Optical observations

At the regional background station SDZ, the aerosol scattering coefficient (σ_{sp}) was measured by an integrating nephelometer (Model M9003, EcoTech, Australia). The BC aerosol concentration was measured with an aethalometer (Model AE31, Magee Scientific, USA). The AE31 Aethalometer measured the optical attenuation of light from LED lamps with seven different wavelengths (370, 470, 520, 590, 660, 880, and 950 nm) transmitted through the aerosols deposited continuously on a quartz fiber filter. The attenuation of light is converted to the BC mass concentration using wavelength dependent calibration factors as recommended by the manufacturer. The light absorption coefficient (σ_{ap}) was indirectly calculated with the BC concentration by the method introduced below. The detail working principle and maintenance of the instruments has been discussed in previously (Zhao et al., 2011; Yan et al., 2009).

An Aerosol lidar (ALS300, EZ manufactured by Leosphere) has was employed in this field campaign at SDZ. The lidar system is based on 355 nm Nd:YAG pulsed laser operating at 16 mJ with 20 Hz repetition rate. The backscattered light is collected by an optical system and its intensity is measured by a photo-detector. The amount of the collected optical radiation is converted into an electronics signal and stored onto a computer. The lidar continuously operated with 30 min intervals and 15 m height resolution. The maximum range is about 20 km. The backscatter and extinction coefficient profiles are retrieved using the well known Klett-Fernald-Sasano evaluation approach used with an assumption of so-called Lidar Ratio (Klett, 1981, 1985; Fernald, 1984). The aerosol optical depth integrated over the maximum of the available lidar range.

2.2 Chemical analysis

Each polypropylene and blank filter was cut into fragments and digested with 16 mL concentrated HNO_3 and 4 mL concentrated $HClO_4$ in a conical flask, and then heated until there was ~3 mL residual left. After cooling, the solution was filtered, and then diluted to 15 mL with ultrapure water. A total of 16 elements (Al, As, Ba, Ca, Cd, Co,

ACPD
13, 903–933, 2013

Cu, Fe, K, Mg, Mn, P, Pb, Sr, Ti and Zn) were analyzed by inductively coupled plasma spectroscopy and atomic emission spectroscopy (ICP-AES)((Model: ULTIMA, JOBIN-YVON Company, France).

One fourth of each quartz fiber filter was put into a glass tube and 10 mL de-ionized water was added. After 15 min ultrasonic bath at room temperature, the solution was drawn into a 5 mL syringe, filtered by a syringe filter, and injected into a polymeric vial with filter cap. The polymeric vials were put into a Dionex AS-DV Autosamplers and analyzed by an ion chromatography (ICS-1000, DIONEX) for water-soluble ions (Na^+, NH_4^+, K^+, Mg^{2+}, Ca^{2+}, Cl^-, NO_3^-, and SO_4^{2-}).

A 0.5 cm^2 punch from each quartz-fiber filter was analyzed by a thermal optical carbon analyzer (DRI-2001A) for eight carbon fractions, following the IMPROVE_A protocol (Chow et al., 1997, 2001, 2007).

2.3 Methods for aerosol absorption coefficient (σ_{ap}) calculation

Aerosol light absorption coefficient (σ_{ap}) can be directly calculated from the attenuation measured by the Aethalometer or indirectly calculated based on the BC concentrations recorded by the instrument. The detailed calculation method has been described in Yan et al. (2008). In this work, the indirect method was employed to calculate the σ_{ap} based on the following equation:

$$\sigma_{ap} = \alpha \times [BC] \quad (1)$$

where, α is the conversion factor or the BC absorption efficiency, and adopted as 8.28 mg m^2 in this work. This value had been used as the conversion factor in previous work at SDZ station (Yan et al., 2009).

2.4 The meteorological data

The meteorological data, mainly the visibility over China, was obtained from the China Meteorological Administration (CMA). The hourly meteorological data, wind direction,

ACPD
13, 903–933, 2013

wind speed, relative humidity (RH), temperature and pressure were measured and recorded every 1 h at SDZ station. Visibility was monitored with a forward scattering measuring visibility meter (Model FD 12, Vaisala Corporation, Finland) at SDZ. In Beijing urban area, the wind profile with time resolution 5 min was observed with a boundary layer wind profile lidar. The profile's range is 3500 m with 50 m vertical resolution. Sounding data observed in Beijing was used to analyze the vertical structure of temperature in this work.

3 Results and discussion

3.1 Meteorological condition and pollutant concentrations

In winter, the NCP region is often dominated by cold high pressure system with low surface wind speeds, sometimes also accompanied by surface temperature inversion. Those conditions are favourable for the formation of haze or fog, and usually lead to high levels of pollutants concentration due to weak mixing and dispersion (Xu et al., 2011).

A surface weak high-pressure system persisted from 16 to 18 January 2010 in Beijing and surrounding area and was replaced by a low-pressure system until 20 January. This weather condition was unfavorable for the dispersion of pollutants. The weather system was finally terminated by the Mongolia anticyclone with strong northerly wind on 20 January (Fig. 2). Under this synoptic condition, winds at the surface were very weak with the wind speed lower than 3.0 $m s^{-1}$ at SDZ and even lower in Beijing urban areas (lower than 2.0 $m s^{-1}$). Both the temperature and relative humidity (RH) showed evident diurnal variation. The temperature increased continuously day by day, and the RH remained high. The surface pressure persistently decreased during this episode. The weak winds and lower pressure were unfavorable for the dispersion of pollution, which caused the accumulation of pollutants on a regional scale. As shown in Fig. 3, the particulate and gaseous pollutants (Fig. 3d–f) increased continuously from 16 to 18

ACPD
13, 903–933, 2013

January at three sites, while they decreased at TJ and BJ, and increased obviously at SDZ on 19 January. The concentrations of $PM_{2.5}$ and CO at BJ and TJ were evidently higher than that at SDZ. The highest concentration of $PM_{2.5}$ was 445.6 $\mu g\,m^{-3}$ and 318.1 $\mu g\,m^{-3}$ at TJ and BJ, respectively. The concentration of CO exceeded 10 ppm at TJ and BJ. The NO_2 increased simultaneously at threes sites and showed significant diurnal variation at SDZ. The average concentrations of $PM_{2.5}$, NO_2 and CO in haze days were 5 ~ 8, 2 ~ 6 and 3 ~ 5 times as high as that in normal days. The sharp increase of pollutants at SDZ on 19 January was mainly attributed to the regional transport, which will be discussed as a part of this study in the following section.

3.2 Light extinction effect of aerosol in this episode

Visibility as a standard meteorological parameter is regularly measured at synoptic meteorological stations all over the world. Since it is determined mostly by the light extinction by aerosol particles, this parameter can be considered as a good indicator of air pollution (Molnár et al., 2008). The standard visibility measurements are carried out under ambient relative humidity (RH), and strongly depend on the available atmospheric water vapor due to the hygroscopic growth of the particles. Consequently, the extinction effect of a given, dry aerosol volume concentration should be separated from that due to hygroscopic growth of the particles via adsorbed water vapor. The noon visibility data has been widely used to examine the spatial-temporal haze trends in the United States (Husar and Wilson, 1993; Schichte et al., 2001). Zhao et al. (2011) pointed out that it was better to quantify haze days with the meteorological observation data at 14:00 (visibility and RH) after comparison two methods of distinguishing haze days with daily mean and 14:00 meteorological data in the BTH area. Therefore, the visibility observed at 14:00 was employed in this study to reflect the aerosol extinction effect in regional scale. The visibility data was obtained from the China Meteorological Administration (CMA). As showed in Fig. 4, the area with visibility lower than 10 km mostly appeared in south of China on 16 January, especially in Sichuan basin, and

ACPD
13, 903–933, 2013

then the area gradually expanded northward, and covered most region of east China including Beijing and Tianjing on 19 January, finally shifted to the south on 20 January driven by the strong northerly winds. Corresponding to the visibility variation, the weather phenomenon observed in the low visibility area was mainly haze at 14:00 from 16 to 18 January, mist was observed and began to increase on 19 January. The haze phenomenon recorded in daytime suggested that the aerosol loading was high enough in this episode to extinct the light and then caused low visibility. These hygroscopic aerosol particles accompanied with increased RH resulted in the lower visibility ultimately, especially during the nighttime.

The extinction by aerosol included scattering and absorption. The observed σ_{sp} and calculated σ_{ap} at SDZ are presented in Fig. 5. The AOD retrieved with the lidar observation is presented as well, which can provide columnar aerosol properties. Similar to the $PM_{2.5}$ concentration, the σ_{sp} and σ_{ap} gradually increased from 16 January to the noon of 18 January, and showed significant diurnal variation with high values around evening and low values around noon. The AOD began to increase on 16 January and gradually increased in the following two days. There was no obvious diurnal variation observed in AOD. All the three parameters increased significantly on the afternoon of 18 January and reached their maxima on 19 January with values of 1430.1 km^{-1}, 219.4 km^{-1} and 2.1 for σ_{sp}, σ_{ap} and AOD, respectively. In this period, the lidar captured several high values of AOD (above 1.5) in the end of the haze episode though the values of AOD were missing in most time due to the presence of cumulus clouds at the top of the PBL. The annual average AOD at 550 nm of Beijing was 0.8 derived from MODIS dataset (Xu et al., 2011). The increased AOD indicated that the aerosol loading in the vertical direction was also increased significantly on 19 January. In haze days, the average values of σ_{sp} and σ_{ap} were 577.3 Mm^{-1} and 55.6 Mm^{-1}, and were 8.1 and 5.2 times as high as that in normal days, respectively. Compared with the seasonal average of σ_{sp} in winter 176 km^{-1} observed at SDZ in 2008, the σ_{sp} averagely increased 2.3 times in haze days (Zhao et al., 2011b). However, the mean σ_{sp} and σ_{ap} were lower than that observed at Wuqing (a site located between BJ and TJ) with values of 742 Mm^{-1}

ACPD
13, 903–933, 2013

and 112 Mm^{-1} during pollution episode in spring and 874 Mm^{-1} and 85 Mm^{-1} in summer, respectively (Ma et al., 2011). The daily average σ_{sp} and σ_{ap} was 1116.7 Mm^{-1} and 89.4 Mm^{-1} on 19 January, that caused further reduction of visibility. The visibility on this day was mostly lower than 2 km. The rapid increase of aerosol loading at the surface and in the vertical distribution was mostly attributed to the regional transport, which is demonstrated in detail later in this paper.

3.3 Chemical characteristics and secondary formation of this episode

The results of chemical analysis of $PM_{2.5}$ at four sites in Beijing, Tianjing and HeBei province are presented in this section to identify the chemical characteristics of the aerosol during this haze episode and discuss secondary formation. The sampling of $PM_{2.5}$ was missed at SJZ during this episode and not analyzed in this paper.

The dust matter in $PM_{2.5}$ was calculated as the sum of oxides of aluminum, calcium, iron, titanium, magnesium and silicon (i.e., mineral dust = 1.89Al + 2.14Si + 1.4Ca + 1.43Fe + 1.66Mg + 1.67Ti) based on our measurement of the concentration of these elementals (Taylor and Mclennan, 1985; Hueglin et al., 2005). The concentration of Si was estimated according to the average ratio of Si/Al (3.9) obtained from Zhang et al. (2003). Organic material (OM) was obtained by multiplying OC concentrations by a factor of 1.2, accounting for hydrogen and oxygen in the organic compounds. This conversion factor had been used in previous work in Beijing (Sun et al., 2004). The results showed that the $PM_{2.5}$ concentration increased sharply during the haze episode. The SO_4^{2-}, NO_3^-, NH_4^+, OM, dust matter, and element carbon were the six dominant species in $PM_{2.5}$ at fours sites in both haze days (16–19 January) and normal days (all days except the haze days from 14 to 23 January) (Fig. 6). However, the secondary inorganic pollutants (SO_4^{2-}, NO_3^- and NH_4^+) and OM increased evidently during the haze episode and became dominated components of $PM_{2.5}$. The total concentrations of SO_4^{2-}, NO_3^- and NH_4^+ exhibited the highest levels during this episode with the average value of 127.0 $\mu g\,m^{-3}$,

ACPD
13, 903–933, 2013

113.5 $\mu g\,m^{-3}$, 56.9 $\mu g\,m^{-3}$ and 46.2 $\mu g\,m^{-3}$ at TJ, BJ, SDZ and CD, respectively. The three components together accounted for 44.8 %, 37.7 %, 41.9 % and 20.1 % of $PM_{2.5}$ mass concentration at TJ, BJ, SDZ and CD, respectively. The concentration of those components on haze days was about 4.3 ~ 9.1 times higher than that on normal days at the four sites, and was significantly higher in large cities Beijing and Tianjin than that in regional background area (SDZ) and in the city to the north of Hebei province (CD) on haze days. However, the percentages were comparable at threes sites in the North China Plain, and considerably higher than that at CD site. The increase of secondary inorganic pollutants had been observed in pollution haze in several cities in east China (Sun et al., 2006; Wang et al., 2006; Tan et al., 2009; Li et al., 2011; Huang et al., 2012). This phenomenon was observed simultaneously at four sites in regional scale in this study, which could be identified as a common characteristic of pollution haze in eastern China.

The higher contribution of sulfate and nitrate in haze episode could be related to high oxidation rates of SO_2 and NO_2. Previous studies have indicated that sulfur oxidation ratio SOR = $n\mathrm{SO}_4^{2-}/(n\mathrm{SO}_4^{2-} + n\mathrm{SO}_2)$ (n refers to molar concentration) and nitrogen oxidation ratio NOR = $n\mathrm{NO}_3^-/(\mathrm{nNO}_3^- + n\mathrm{NO}_2)$ can be used to estimate the degree of secondary formation of nitrogen and sulfur (Sun et al., 2006; Wang et al., 2006). As showed in Table1, the average values of SOR and NOR were 0.16 and 0.40 on haze days at TJ and about 1.50 and 1.14 times higher than that on normal days, respectively. At BJ, both SOR and NOR on haze days with values 0.29 and 0.51 were about 1.8 times as much as that in the normal days. The increased SOR and NOR on haze days indicated the effect of secondary formation. The conversion of SO_2 to sulfate was mainly attributed to the gas-phase oxidation by OH and H_2O_2 radical or heterogeneous oxidation (Seinfeld et al., 1986; Calvert et al., 1985). Many studies suggested that the conversion of SO_2 to sulfate in winter haze was more significant through the aqueous phase oxidation of SO_2 by the catalysis of the transition metals instead of the gas-phase oxidation (Sun et al., 2006; Tan et al., 2009; Li et al., 2011). Our measurements confirm this view in our study region area. As shown in Fig. 7a, the concentration

ACPD
13, 903–933, 2013

of NO_2 was very high but the O_3 concentration was less than 5 ppb during the haze episode at BJ (TJ was similar as BJ and not showed here). Both of them had no evident diurnal variation. These results suggested that the photochemical activity was very weak in haze period. The high levels of NO_2 and the weak photochemical activity could not produce sufficient conversion oxidants (OH and H_2O_2 radicals) for gas-phase oxidation of SO_2. (Poppe et al., 1993; Hua et al., 2008). The increased relative humidity in haze days (Fig.3) was a favorable factor for the aqueous phase oxidation of SO_2. The formation of nitrate in urban area was probably through the heterogeneous hydrolysis process. By analysis of sulfate, nitrate, and ammonium in $PM_{2.5}$ in four cities in China, Pathak et al. (2009) pointed out that the nitrate was most probably formed via the heterogeneous hydrolysis of N_2O_5 on the surface of the moist and acidic aerosols in Beijing and Shanghai, especially during humid and hazy weather. The formation of nitrate in $PM_{2.5}$ is still less well understood and needs further study in the future. However, the observed results were different at SDZ from that at two urban sites. The NOR was higher in haze days with value of 0.33, while the SOR in haze days 0.16 was lower than 0.23 in normal days. From Fig.7b, it could be found that the NO_2 and O_3 showed obvious diurnal variations with increasing trend from 16 to 18 January. The concentration of O_3 was highest around noon and lowest in the night, which was the typical characteristic of photochemical process. On the last day of the haze, namely 19 January, the variations of NO_2 and O_3 were similar to that at BJ which probably dominated by the regional transport. Thus, the increased sulfate and nitrate at SDZ in haze days maybe attributed to photochemical reaction, regional transport and heterogeneous reaction process. The lower SOR might be attributed to the sharply decrease of SO_2 relative to the decrease of SO_4^{2-} diluted by the strong northerly wind. The SOR and NOR were not calculated at CD due to the absent observation of gases.

During haze episode, the organic material in the $PM_{2.5}$ increased significantly besides sulfate and nitrate, especially evident at CD (Fig. 6). The OC/EC ratio is widely used to identify the presence of secondary organic aerosols when the value exceeds 2.0 (Chow et al., 1994, 1996). From Table 1, it could be found that secondary organic

ACPD
13, 903–933, 2013

aerosols existed in the $PM_{2.5}$ at both haze and normal days at TJ, BJ and SDZ, and increased in haze days with higher OC/EC ratio at TJ and BJ but slightly changed at SDZ. At the north city CD, the OC/EC ratio was lower than 2.0 in normal days but significantly increased to 4.34 in haze days, which suggested that secondary organic aerosols had a greater regional impact during haze episode. The analysis of chemical characteristics of aerosol indicated that the secondary formation of aerosol was one important mechanism in the haze formation.

3.4 Accumulation and transport of pollutants in this episode

As mentioned in Sect. 3.1, this haze episode was caused by a surface high pressure system in the early phase and a low pressure system in the later period. In Fig. 8, the temperature inversion could be found about 800 hPa on 16 January which then strengthened and descended gradually over the following two days. The inversion lowered to the surface on 17 January with the strongest inversion occurring around 900 hPa in the night. The vertical wind presented in Fig. 9 was distinguished by two layers above and below 500 m. The lower layer was mainly distributed under 400 m with low wind speed, and descending air in the whole layer. There was no obvious change in the wind pattern until the afternoon of 18 January. This corresponded to the dominated high pressure system in this period. The descending motion in the lower troposphere forced the aerosol particles into a very shallow layer. With the measurement of lidar (Fig. 10), it could be found that the aerosol particles were mainly concentrated below 500 m during this episode. The maximum of aerosol loading was located around 200 ~ 400 m. The similar vertical distribution of wind and aerosol indicated that the height of PBL was about 400 m. The shallow PBL severely limited pollutant diffusion in the vertical. The weak horizontal wind limited the horizontal dispersion of pollutants that produced very high concentrations in urban area (such as BJ and TJ) and relatively lower concentrations in the more suburban area (SDZ). However, the pollutant concentrations were still elevated above non-episode levels in the suburban area under the large scale stagnation weather condition (Fig. 3d–f). The accumulation of pollutions

ACPD
13, 903–933, 2013

was the main factor in the haze formation in these three days. In the afternoon of 18 January, the controlling synoptic weather over Beijing and surrounding area changed to low pressure system. The southwest wind appeared from surface to 800 m and even stronger in the layer 800 ~ 2000 m, which transported the pollutants from the more southern regions toward the north. Correspondingly, a layer with high aerosol loading located about 800 m to 1000 m was observed at 19:00 on 18 January above the downwind area (Fig.10). Accompanying the strong southwest wind, enhanced descent of air occurred in the whole vertical direction on 19 January, which carried part of pollutants to the ground. At the same time, the surface wind at SDZ turned from east-northeast to southwest in the afternoon of 18 January (Fig. 3a), and carried pollutants to this area that resulted in the highest aerosol loading in the lower aerosol layer on 19 January. The ground and high layer transport of pollutants resulted in the rapidly increase of pollutants in the downwind area, but caused decrease of pollutants in urban area on 19 January (Fig. 3d–f). The regional transport of pollutants expanded geographical extent of the haze. With the arrival of the Mongolia anticyclone, the northerly wind first appeared aloft and diluted pollutants in that layer of the atmosphere. The higher aerosol layer had disappeared at 20:00 on 19 January, while the surface layer still remained with high aerosol loading. 20 January, the aerosol loading near surface decreased significantly and finally the entire polluted volume was diluted and transported by the strong northerly wind that terminated this haze episode.

4 Summary and conclusion

An intensive aerosol and trace gases campaign was carried out over the BTH region in the North China Plain from 14 to 23 January 2010. A regional haze episode occurred during this period. With analysis of the chemical and optical properties of aerosols and the meteorological condition, the formation of this episode was investigated in this study.

ACPD
13, 903–933, 2013

The haze episode occurred from 16 to 19 January 2010, which was mainly caused by a surface high pressure system in most time and a low pressure system in the later period. During this episode, the concentrations of $PM_{2.5}$ and main trace gases increased significantly in regional scale. The area with visibility lower than 10 km covered most region of east China. The haze phenomenon recorded in daytime corresponding to the low visibility suggested that the aerosol loading was high enough in this episode to extinct the light. The increased σ_{sp}, σ_{ap} and AOD further supported the important extinction effect of aerosol in the formation of this haze episode.

The secondary inorganic pollutants (SO_4^{2-}, NO_3^- and NH_4^+) and OM increased evidently during this episode and become dominated components of $PM_{2.5}$. The concentration level of secondary pollutants was significantly higher in large cities than that in regional background area and city in north area of Hebei province, while the percentage was comparable at threes sites in the North China Plain, and evidently higher than that at CD site. The increase of secondary inorganic pollutants was observed simultaneously at four sites, especially in plain area of BTH, which could be identified as a common characteristic of pollution haze in east China.

The sulfate and nitrate in $PM_{2.5}$ were mainly formed through the heterogeneous reaction process at BJ and TJ. At SDZ, the photochemical reaction, regional transport and heterogeneous reaction process probably together caused the increase of sulfate and nitrate. The secondary organic aerosols existed in the $PM_{2.5}$ in both haze and normal days at TJ, BJ and SDZ, while only existed in haze days at CD. The increase of secondary organic aerosols at four sites suggested the greater regional impact during haze episode. The chemical characteristics of aerosols in $PM_{2.5}$ indicated that the secondary formation of aerosol was one important mechanism in the formation of haze episode.

The strong temperature inversion, weak surface wind speed and descending air motions in PBL caused pollutants to accumulate in a shallow layer and produced high pollutant concentrations within the source region. The accumulation of pollutants was one of the main factors in the haze formation. The enhanced southwest wind in the

ACPD
13, 903–933, 2013

entire layer transported pollutants from southern urban to the downwind area in the later period, which expanded the geographical scope of the haze.

Acknowledgement. This work was supported by the National Natural Science Foundation of China (41205121, 41105092), the Beijing Natural Science Foundation (8131003, 8132025, 8121002), the Research Funding of Institute of Urban Meteorology (IUMKY201209), and Special Grant in Atmospheric Sciences Field supported by CMA (GYHY200806027). The authors would like to thank the staff of the Shangdianzi and Chengde station for assisting the measurements. We also thank the editor for his helpful comments and suggestions on the manuscript and polishing the English writing.

References

Calvert, J., Lazrus, A., Kok, G., Heikes, B., Walega, J., Lind, J., and Cantrell, C.: Chemical mechanisms of acid generation in the troposphere, Nature, 317, 27–35, doi:10.1038/317027a0, 1985.

Chow, J., Waston, J., Chen, L., Chang, M., Robinson, N., Trimble, D., and Kohl, S.: The IMPROVE – a temperature protocol for thermal/optical carbon analysis: maintaining consistency with a long-term database, J. Air Waste Manage. Assoc., 57, 1014–1023, 2007.

Chow, J. C., Watson, J. G., Crow, D., Lowenthal, D. H., and Merrifield, T.: Comparison of IMPROVE and NIOSH carbon measurements, Aerosol Sci. Technol., 34, 23–34, 2001.

Chow, J. C., Watson, J. G., Pritchett, L. C., Pierson, W. R., Frazier, C. A., and Purcell, R. G.: The DRI thermal/optical reflectance carbon analysis system: Description, evaluation and application in US air quality studies, Atmos. Environ., 27A, 1185–1201,1993.

Chow, J. C., Watson, J. G., Fujita, E. M., Lu, Z., and Lawson, D. R.: Temporal and spatial variations of $PM_{2.5}$ and PM_{10} aerosol in the southern California air quality study, Atmos. Environ., 28, 3773–3785, 1994.

Chow, J. C., Watson, J. G., Lu, Z., Lowenthal, D. H., Frazier, C. A., Solomom, P. A., Thuiller, R. H., and Magliano, K.: Descriptive analysis of $PM_{2.5}$ and PM_{10} at regionally representative locations during SJVAQS/AUSPEX, Atmos. Environ., 30, 2079–2112, 1996.

Fernald, F. G.: Analysis of atmospheric lidar observations – some comments, Appl. Opt., 23, 652–653, 1984.

ACPD

13, 903–933, 2013

Hua, W., Chen, Z. M., Jie, C. Y., Kondo, Y., Hofzumahaus, A., Takegawa, N., Chang, C. C., Lu, K. D., Miyazaki, Y., Kita, K., Wang, H. L., Zhang, Y. H., and Hu, M.: Atmospheric hydrogen peroxide and organic hydroperoxides during PRIDE-PRD'06, China: their concentration, formation mechanism and contribution to secondary aerosols, Atmos. Chem. Phys., 8, 6755–6773, doi:10.5194/acp-8-6755-2008, 2008.

Huang, K., Zhuang, G., Lin, Y., Fu, J. S., Wang, Q., Liu, T., Zhang, R., Jiang, Y., Deng, C., Fu, Q., Hsu, N. C., and Cao, B.: Typical types and formation mechanisms of haze in an Eastern Asia megacity, Shanghai, Atmos. Chem. Phys., 12, 105–124, doi:10.5194/acp-12-105-2012, 2012.

Hueglin, C., Gehrig, R., Baltensperger, U., Gysel, M., Monnd, C., and Vonmonta, H.: Chemical characteristics of $PM_{2.5}$, PM_{10} and coarse particles at urban, near-city and rural sites in Switzerland, Atmos. Environ., 39, 637–651, 2005.

Husar, R. B. and Wilson, W. E.: Haze and sulfur emission trends in the eastern United States, Environ. Sci. Technol. 27, 12–16, 1993.

Kang, H., Zhu, B., Su, J., Wang, H., Zhang, Q., and Wang, F.: Analysis of a long-lasting haze episode in Nanjing, China, Atmos. Res., 120–121, 78–87, doi:10.1016/j.atmosres.2012.08.004, 2013.

Klett, J. D.: Stable analytical inversion solution for processing Lidar returns, Appl. Opt., 20, 211–220, 1981.

Klett, J. D.: Lidar inversions with variable backscatter/extinction values, Appl. Opt., 24, 1638–1643, 1985.

Li, W. J., Shao, L. Y., and Buseck, P. R.: Haze types in Beijing and the influence of agricultural biomass burning, Atmos. Chem. Phys., 10, 8119–8130, doi:10.5194/acp-10-8119-2010, 2010.

Li, W. j., Zhou, S. , Wang, X., Xu, Z., Yuan, C., Yu,Y., Zhang, Q., and Wang, W.: Integrated evaluation of aerosols from regional brown hazes over northern China in winter: Concentrations, sources, transformation, and mixing states, J. Geophys. Res., 116, D09301, doi:10.1029/2010JD015099, 2011.

Ma, N., Zhao, C. S., Nowak, A., Müller, T., Pfeifer, S., Cheng, Y. F., Deng, Z. Z., Liu, P. F., Xu, W. Y., Ran, L., Yan, P., Göbel, T., Hallbauer, E., Mildenberger, K., Henning, S., Yu, J., Chen, L. L., Zhou, X. J., Stratmann, F., and Wiedensohler, A.: Aerosol optical properties in the North China Plain during HaChi campaign: an in-situ optical closure study, Atmos. Chem. Phys., 11, 5959–5973, doi:10.5194/acp-11-5959-2011, 2011.

ACPD
13, 903–933, 2013

Molnár, A. Mészáros, E., Imre, K., and Rüll, A.: Trends in visibility over Hungary between 1996 and 2002, Atmos. Environ., 42, 2621–2629, 2008.
Parrish, D. D. and Zhu, T.: Clean air for megacities, Science, 326, 674–675, doi:10.1126/science.1176064, 2009.
Poppe, D., Wallasch, M., and Zimmermann, J.: The dependence of the concentration of OH on its precursors under moderately polluted conditions: a model study, J. Atmos. Chem., 16, 61–78, 1993.
Schichte, B. A., Husar, R. B., Falke, S. R., and Wilson, W. E.: Haze trends over the United States, 1980–1995, Atmos. Environ., 35, 5205–5210, 2001.
Seinfeld, J. H.: Atmospheric Chemistry and Physics of Air Pollution, Wiley, New York, 1986.
Sun, Y., Zhuang, G., Wang, Y., Han, L., Guo, J., Dan, M., Zhang, W., Wang, Z., and Hao, Z.: The air-borne particulate pollution in Beijing-concentration, composition, distribution and sources, Atmos. Environ., 38, 5991– 6004, 2004.
Sun, Y., Zhuang, G., Tang, A.,Wang, Y., and An, Z.: Chemical characteristics of $PM_{2.5}$ and PM_{10} in haze-fog episodes in Beijing, Environ. Sci. Technol. 40, 3148–3155, 2006.
Tan, J. H., Duan, J. C., Chen, D. H., Wang, X. H., Guo, S. J., Bi, X. H., Sheng, G. Y., He, K. B., and Fu, J. M.: Chemical characteristics of haze during summer and winter in Guangzhou, Atmos. Res., 94, 238–245, 2009.
Taylor, S. R. and Mclennan, S. M.: The Continental Crust: its Composition and Evolution, Blackwells, Oxford, England, 1985.
Wang, Y., Zhuang, G., Sun, Y., and Zheng, A.: The variation of characteristics and formation mechanisms of aerosols in dust, haze, and clear days in Beijing, Atmos. Environ., 40, 6579–6591, 2006.
Wang, X., Wang,W., Yang, L., Gao, X., Nie, W., Yu, Y., Xu, P., Zhou,Y., and Wang,Z.: The secondary formation of inorganic aerosols in the droplet mode through heterogeneous aqueous reactions under haze conditions, Atmos. Environ., 63, 68–76, 2012.
Xu, W. Y., Zhao, C. S., Ran, L., Deng, Z. Z., Liu, P. F., Ma, N., Lin, W. L., Xu, X. B., Yan, P., He, X., Yu, J., Liang, W. D., and Chen, L. L.: Characteristics of pollutants and their correlation to meteorological conditions at a suburban site in the North China Plain, Atmos. Chem. Phys., 11, 4353–4369, doi:10.5194/acp-11-4353-2011, 2011.
Zhang, X. Y., Gong, S. L., Shen, Z. X., Mei, F. M., Xi, X. X., Liu, L. C., Zhou, Z. J., Wang, D., Wang, Y. Q., and Cheng, Y.: Characterization of soil dust aerosol in China and its transport

ACPD
13, 903–933, 2013

and distribution during 2001 ACE-Asia: 1. Network observations, J. Geophys. Res., 108, 4261, doi:10.1029/2002JD002632, 2003.

Zhao, P. S., Zhang, X. L., Xu, X. F., and Zhao, X. J.: Long-term visibility trends and characteristics in the region of Beijing, Tianjin, and Hebei, China, Atmos. Res., 101, 711–718, 2011a.

Zhao, X. J., Zhang, X. L., Pu, W. W., Meng, W., and Xu, X. F.: Scattering properties of the atmospheric aerosol in Beijing, China, Atmos. Res., 101, 799–808, 2011b.

Zhao, X. J., Zhang, X. L., Xu, X. F., Xu, J., Meng, M., and Pu, W. W.: Seasonal and diurnal variations of ambient $PM_{2.5}$ concentration in urban and rural environments in Beijing, Atmos. Environ., 43, 2893–2900, 2009.

ACPD

13, 903–933, 2013

Table 1. SOR, NOR and OC/EC during haze days and normal days at four sites.

	TJ			BJ			SDZ			CD		
	SOR	NOR	OC/EC	SOR	NOR	OC/EC	SOR	NOR	OC/EC	SOR	NOR	OC/EC
HD	0.16	0.40	4.40	0.29	0.51	4.53	0.16	0.33	4.09	N	N	4.34
ND	0.06	0.19	3.00	0.16	0.28	3.27	0.23	0.20	4.47	N	N	1.72
Ratio	2.50	2.14	1.47	1.81	1.78	1.39	0.69	1.67	0.91	N	N	2.52

HD: haze days; ND: normal days; ratio: the ratio of values in HD to that in ND; N: no data.

ACPD
13, 903–933, 2013

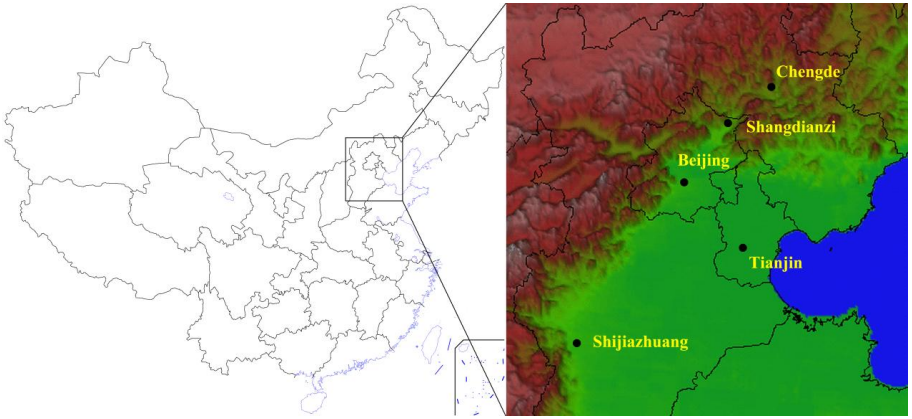

Fig. 1. Sampling sites of $PM_{2.5}$.

ACPD
13, 903–933, 2013

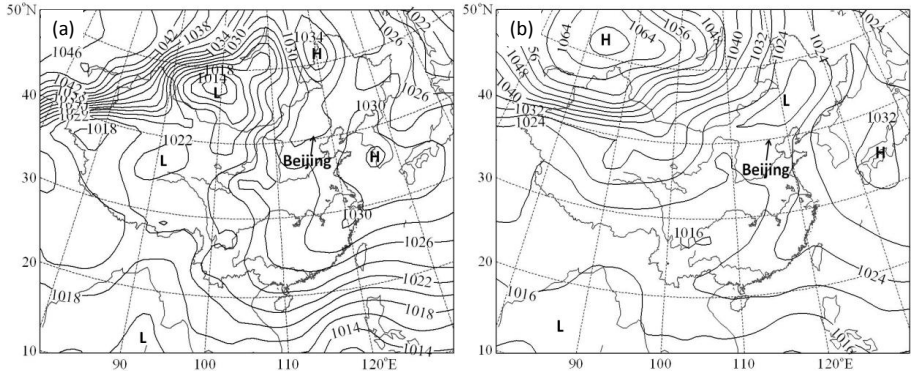

Fig. 2. Surface weather patterns at 08:00 LT on **(a)** 18 January 2012 and **(b)** 19 January 2012.

ACPD
13, 903–933, 2013

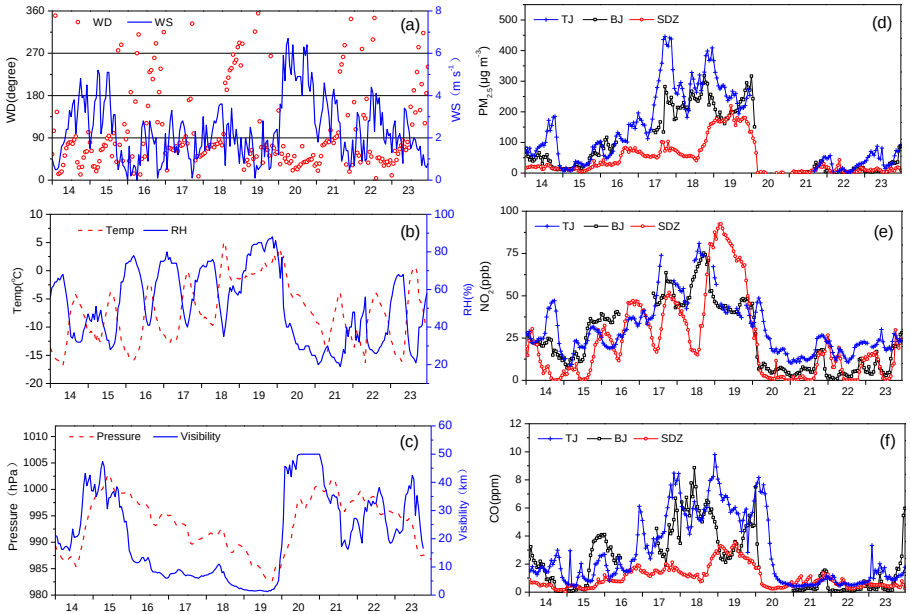

Fig. 3. Time series variations of meteorological parameters at SDZ and pollutants at TJ, BJ and SDZ from 14 to 23 January 2010. **(a)** wind direction and wind speed ($m\,s^{-1}$), **(b)** temperature (°C) and relative humidity (%), **(c)** atmospheric pressure (hPa) and visibility (km), **(d)** $PM_{2.5}$ concentration ($\mu g\,m^{-3}$), **(e)** NO_2 (ppb), **(f)** CO (ppb).

ACPD
13, 903–933, 2013

Analysis of a winter regional haze event and its formation mechanism

X. J. Zhao et al.

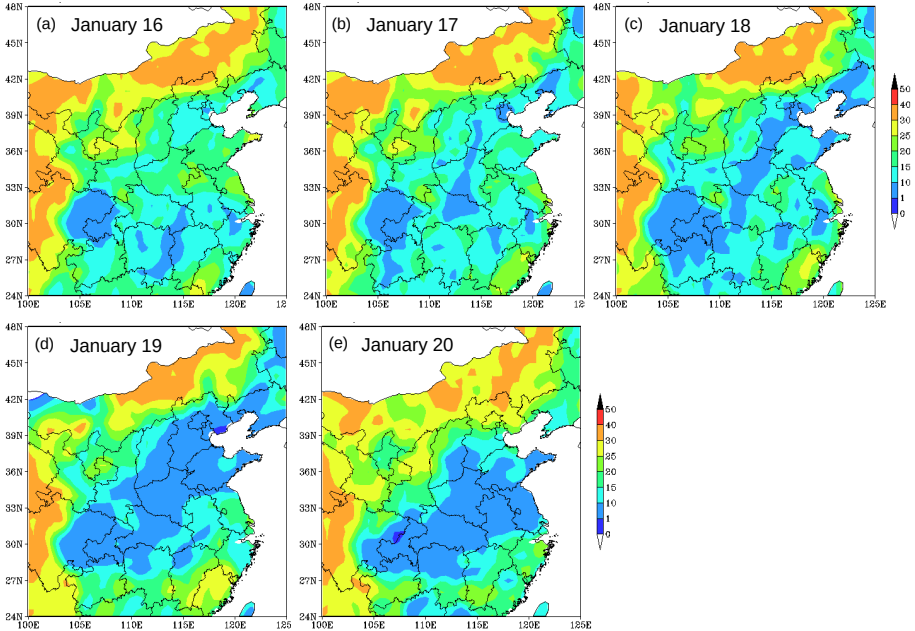

Fig. 4. Regional distribution of visibility (km) at 14:00 LT during 16–20 January.

ACPD
13, 903–933, 2013

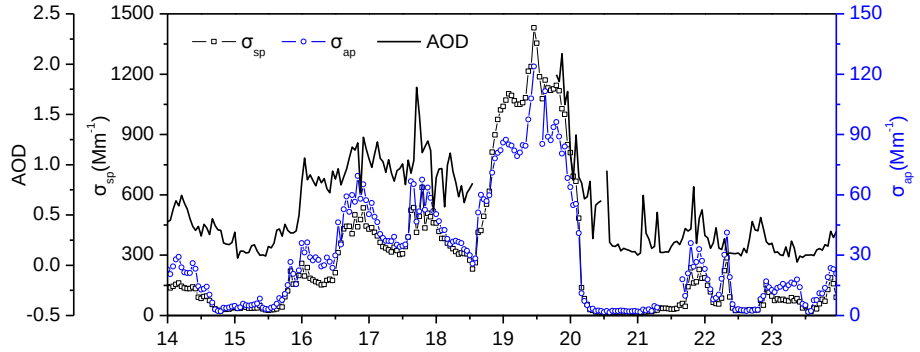

Fig. 5. Time series of aerosol scattering (σ_{sp}), absorption coefficient (σ_{ap}) and aerosol optical depth (AOD).

ACPD
13, 903–933, 2013

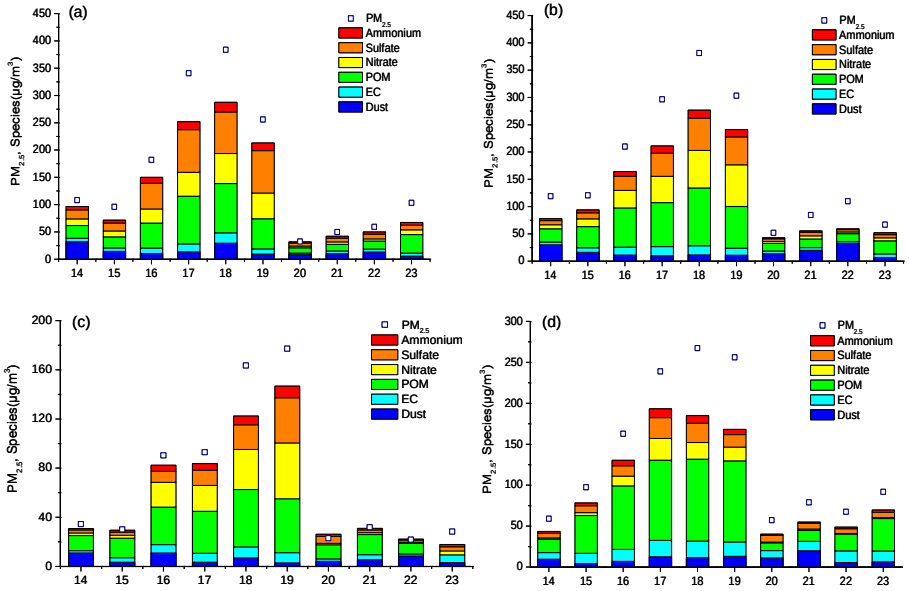

Fig. 6. Variation of concentrations of $PM_{2.5}$ and chemical species at **(a)** TJ, **(b)** BJ, **(c)** SDZ and **(d)** CD.

ACPD
13, 903–933, 2013

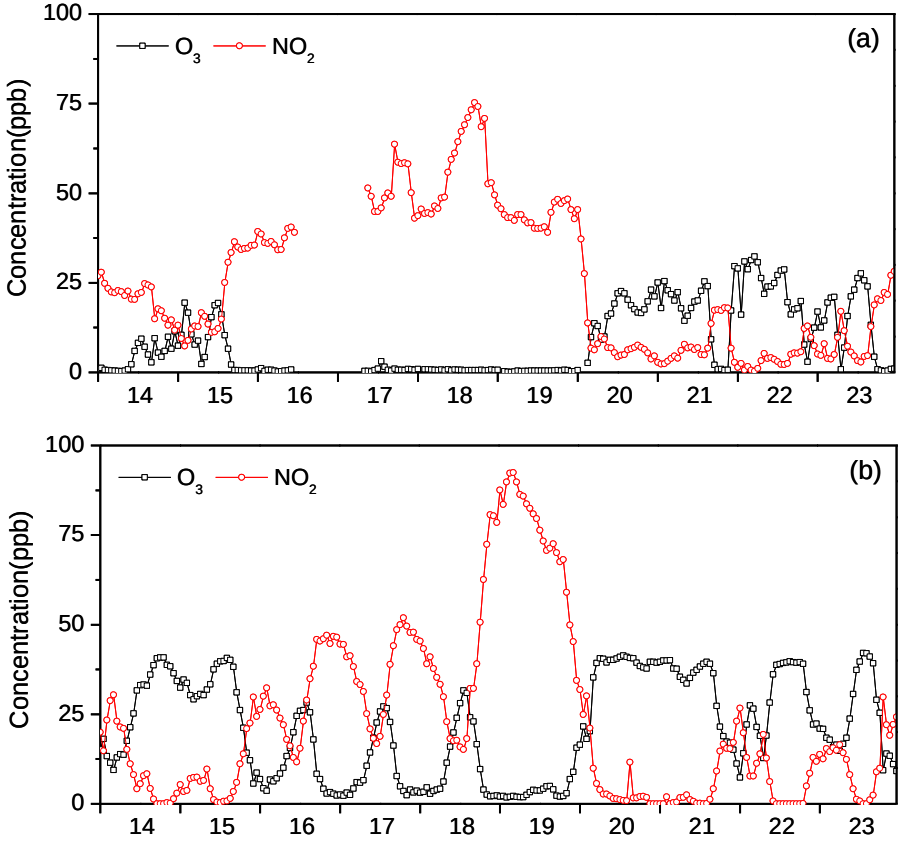

Fig. 7. Time series variations of O_3 and NO_2 at **(a)** BJ and **(b)** SDZ.

ACPD
13, 903–933, 2013

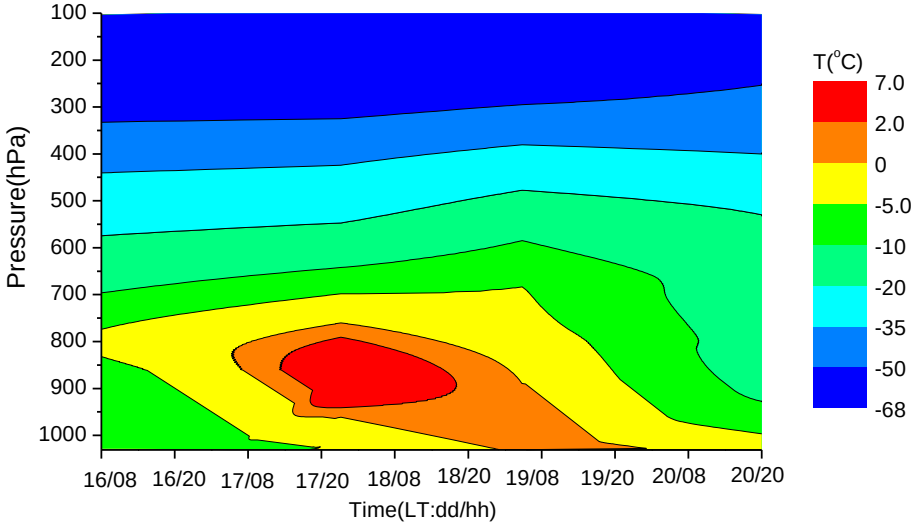

Fig. 8. Variation of temperature in vertical direction.

ACPD
13, 903–933, 2013

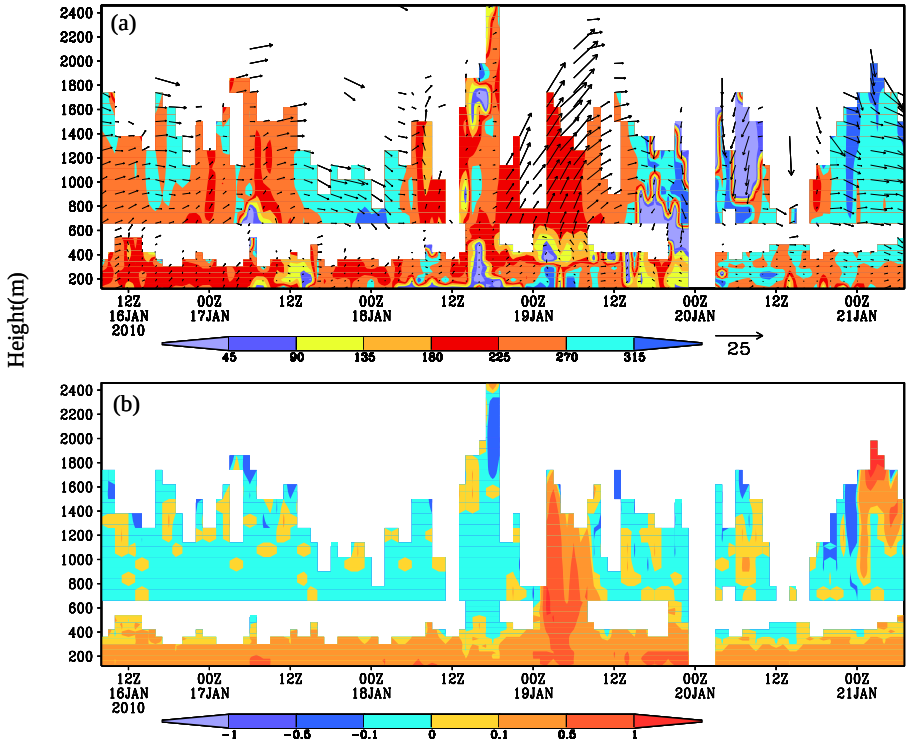

Fig. 9. The lidar measurement of wind profile in Beijing region from 16 to 21 January. **(a)** horizontal wind vectors and wind direction (shaded); **(b)** vertical winds ($m\,s^{-1}$).

ACPD
13, 903–933, 2013

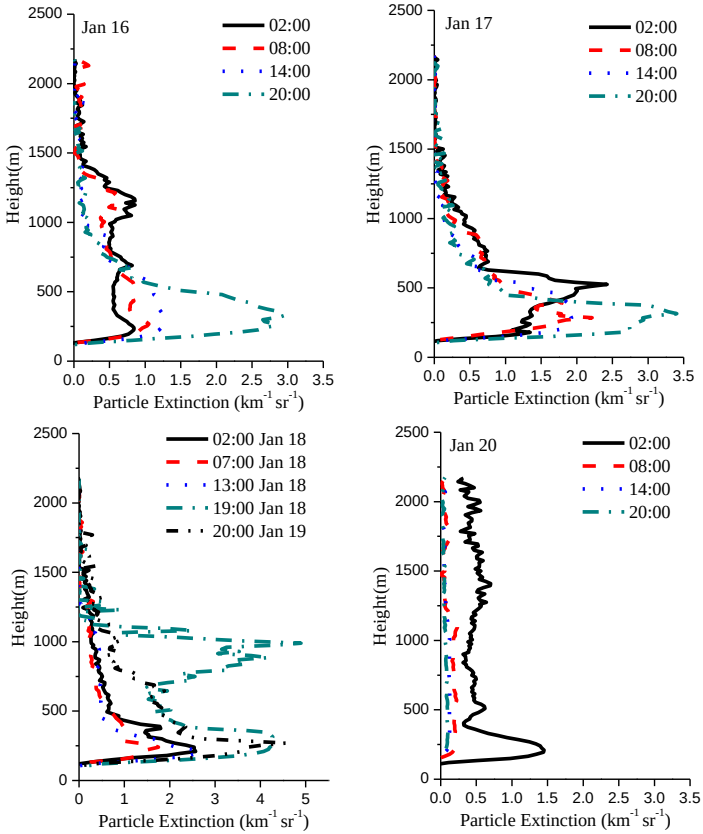

Fig. 10. Vertical profile of particle extinction from 16 to 20 January.

ACPD
13, 903–933, 2013